Available online at www.sciencedirect.com
ScienceDirect
Sensors and Actuators A 135 (2007) 731–739
SENSORS AND ACTUATORS A PHYSICAL
www.elsevier.com/locate/sna

Thermal analysis for bulk-micromachined electrothermal hydraulic microactuators using a phase change material

Jun Su Lee *, Stepan Lucyszyn

Optical and Semiconductor Devices Group, Department of Electrical and Electronic Engineering, Imperial College London, Exhibition Road, London SW7 2AZ, United Kingdom

Received 6 February 2006; received in revised form 14 June 2006; accepted 29 July 2006
Available online 12 September 2006

Abstract

Paraffin wax has been exploited in microactuators because it exhibits a volumetric expansion of ∼15%, at around its melting point. In order to understand paraffin wax actuation, for the first time, the melting process has been investigated using a combination of analytical modelling (using Stefan's problem and Neumann's solution), finite element method (FEM) simulations and actuation data from measurements of a Braille cell and micropipette. This approach gives information on the location of the melting front (interface) at a given melting time, and on the temperature profiles in the paraffin wax during melting. Using the measured actuation response times of approximately 42 and 10 s for the Braille cell and the micropipette, temperatures for the infinitesimally thin layer of theoretical liquid paraffin wax are calculated at approximately 80 and 110 °C, respectively. These calculated temperatures for the infinitesimally thin layer of liquid paraffin wax are reasonable, when considering the real melting process within the microactuator. Using FEM simulations, the melting process was simulated and the final melting times were found to be almost identical to the analytical results. The results from the analytical method closely resemble the natural behaviour of the real melting process. This analytical modelling of the melting process can provide useful information for designing optimal electrothermal hydraulic microactuators using phase change materials (PCMs) and their operating actuation characteristics.

Keywords: Melting process; Microactuator; Paraffin wax; Stefan's problem; Neumann's solution

1. Introduction

Phase change materials (PCMs) have the property of volumetric expansion when changing from solid to liquid (or liquid to gas) phases. Generally, this expansion can produce large hydraulic pressures that can be exploited to realize useful electrothermal microactuators.

As a PCM, paraffin wax is a suitable material for generating large hydraulic forces by means of phase changing. When paraffin wax melts, a volumetric expansion of ∼15% occurs. Since this expansion produces a large hydraulic pressure, it has been investigated for applications in macroactuators [1,2] and microactuators [3]. In recent years, micromachined paraffin wax microactuators [4–7] and paraffin-actuated microvalves [8,9] have also been studied. Recently, Hjort's group at Uppsala University fabricated microfluidic systems, such as a micropump, microvalve and microneedle, using paraffin wax microactuators [10–12]. In addition, a refreshable Braille cell actuated using paraffin wax microactuators has been developed for Braille displays [13].

In addition, this paraffin wax microactuator has also been applied to microfluidic bulk-micromachined microvalves, micropipettes and microgrippers [14,15].

Previous research on the electrothermal hydraulic microactuator using a PCM has focused on experimental techniques for fabricating such devices. Analysis of the melting process for paraffin wax in microactuators is required to optimally design and control the microactuators. Unfortunately, measuring the melting process directly, using thermocouples or thermometers, may be impractical within micro-scale actuators. For these reasons, an analytical modelling method can provide useful information for investigating the melting processes and for predicting the actuation response time of the microactuator.

In this paper, the paraffin wax melting process is analyzed for previously fabricated microactuators employed within a

* Corresponding author. Tel.: +44 20 7594 6294; fax: +44 20 7594 6308.
E-mail addresses: jun-su.lee@imperial.ac.uk (J.S. Lee), s.lucyszyn@imperial.ac.uk (S. Lucyszyn).

0924-4247/$ – see front matter © 2006 Elsevier B.V. All rights reserved.
doi:10.1016/j.sna.2006.07.033

refreshable Braille cell and a micropipette. Here, analytical modelling of the melting process is performed using the two-phase Stefan's problem, by considering the effect of density change on a semi-infinite slab of paraffin wax [16]. The melting rate and temperature profiles for the paraffin wax during melting are calculated using the measured actuation times of the refreshable Braille cell and the micropipette.

2. Microactuators for the Braille cell and micropipette

Since the microactuator for the Braille cell [13] is of a similar design, only the version for the micropipette will be described here. The basic construction of the paraffin wax microactuators and the micropipette are illustrated in Fig. 1. The electrothermally controlled microactuator exploits the hydraulic pressure due to the volumetric expansion of melted paraffin wax. The microactuator consists of a gold microheater on a glass (Pyrex) substrate, silicon bulk-micromachined paraffin wax container and polydimethylsiloxane (PDMS) diaphragm on the top. The PDMS diaphragm is shaped into a hemispherical dome when the microactuator is activated. If the microactuator is required for a specific height (or displacement), the solid phase volume of paraffin wax and the container dimensions can be calculated using the paraffin wax volumetric expansion of ~15%. The high density microheater covers the entire underside of the paraffin wax on the floor of the container. The microheater can generate sufficient thermal energy, through joules heating.

2.1. Experimental results

A new concept for the realization of a refreshable Braille cell has been presented [13]. The complete 3 × 2 dot Braille cell has air gaps between containers, to prevent unwanted actuation by means of heat leakage from adjacent containers. The prototype Braille cell measures 7 mm × 8.5 mm × 2 mm. The

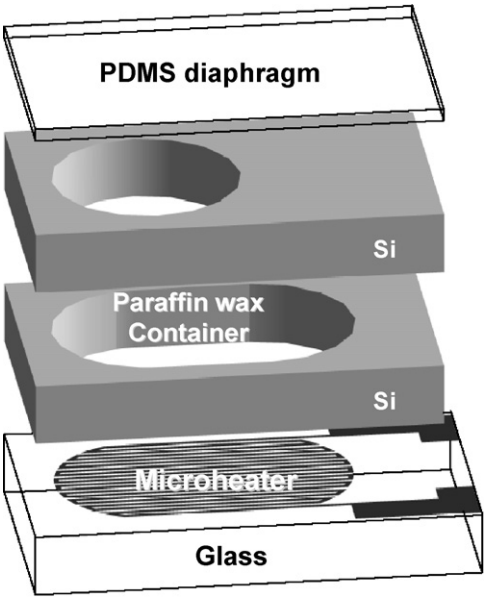

Fig. 1. Exploded view of the basic bulk-micromachined microactuator.

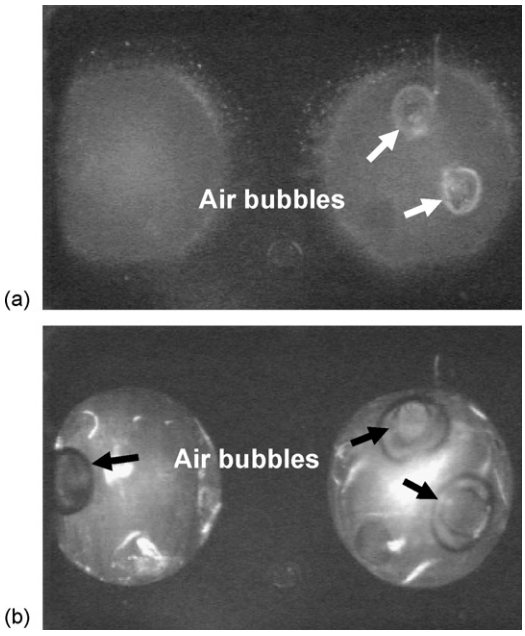

Fig. 2. Two of the four microactuators within the micropipette: (a) before actuation and (b) fully activated after 10 s at 10 V DC.

actuation response time for a dot was ~42 s with a 10 V DC bias voltage, to reach the designed actuation height of 500 μm.

Fig. 2 shows the actuation of the fabricated micropipette (two out of the four internal microactuators can be seen). The actuation response time was about 10 s with a 10 V DC bias voltage, to reach the designed actuation height of 500 μm. With both experimental results, the bias voltages are DC only.

3. Thermal analysis

The actuation response time of the microactuation is determined by the melting rate of the paraffin wax. This melting rate is affected by the volume and thermal properties (e.g. melting point, specific heat, thermal conductivity and latent heat) of the paraffin wax. Given the thermal properties and the measured melting time of the paraffin wax, the melting process within the microactuator can be analyzed. This analytical modelling for PCM was developed for thermal energy storage systems, since the melting and solidification of the PCM accompany heat exchange. The phase changing process is dependent on the thermal conduction, convection, diffusion and thermal properties of the PCM.

3.1. Stefan's problem and Neumann's solution

The melting process within a PCM is a transient and non-linear phenomenon with a moving solid–liquid interface, referred to as the moving boundary problem. The best known analytical modelling method for a one-dimensional moving boundary problem is Stefan's problem that is extended by Neumann [16]. The classical Stefan's problem is a pure conduction problem with a constant end-wall temperature boundary condition. After melting has been started ($t > 0$), the PCM can be

divided into the liquid phase, solid phase and the interface between them. The thermal status of these three areas are important factors for analytical modelling of the PCM. Initially, Stefan solved the simplest one-phase problem. The Stefan's phase change problem is based on the so-called Stefan's condition:

$$\rho L X' = [\vec{q} \cdot \vec{n}]_{\text{solid}}^{\text{liquid}}, \text{ on the interface} \quad (1)$$

where ρ is the density, L the latent heat, X' the normal component of the velocity of the moving interface and $\vec{q} \cdot \vec{n}$ is the heat flux normal to the moving interface between liquid and solid. Stefan's condition states that the latent heat released, due to the interface displacement, equals the net amount of heat transferred from the interface per unit area per unit time. Thus, according to the energy conservation law, Stefan's condition is a statement of heat balance across the interface.

With this one-phase problem, the liquid phase has a higher temperature (T_l) than its melting point (T_m), the solid phase and interface area are assumed to stay at the melting temperature of the PCM in a semi-infinite region. Neumann extended Stefan's problem to a two-phase problem. In this more realistic scenario, the initial state of the PCM is assumed to be solid. With the melting process, the initial temperature of the solid is at a temperature (T_s) below the melting point (T_m) of the PCM, and its temperature during melting is not maintained at a constant value. With Stefan's problem, having constant thermophysical properties, the rate of melting or solidification in the semi-infinite region is governed by a dimensionless number, known as the Stefan number (St) [16],

$$St_l = \frac{c_l(T_l - T_m)}{L}, \qquad St_s = \frac{c_s(T_m - T_s)}{L} \quad (2)$$

where St_l and St_s are Stefan's numbers for the liquid and solid, c_l and c_s the heat capacities of the liquid and solid, L the latent heat of fusion, and T_l, T_s and T_m are the temperatures of the liquid, solid phase and melting point, respectively. In this research, the two-phase Stefan's problem, considering the effect of density change (expansion, $\rho_l < \rho_s$) on a semi-infinite slab of paraffin wax, is exploited in order to analyze the melting processes of paraffin wax within the microactuator.

The initial condition for this solution is:

$$T(x, 0) = T_s < T_m \text{ for } x > 0, X(0) = 0$$

where x is the distance and X is the interface location.

And the boundary conditions are:

$$T(0, t) = T_l > T_m \text{ for } t > 0$$

$$T(x, t) = T_s \text{ for } x \to \infty, t > 0$$

where t is time.

Neumann's solutions give interface (i.e. melting front) location (X) at time (t) after melting:

$$X(t) = 2\lambda\sqrt{\alpha_l t}, \quad t > 0 \quad (3)$$

where α_l is the thermal diffusivity of the liquid phase. The temperature in liquid region ($0 < x < X(t)$, $t > 0$) is obtained using:

$$T(x, t) = T_l - (T_l - T_m)\frac{\text{erf}(x/(2\sqrt{\alpha_l t}))}{\text{erf}(\lambda)} \quad (4)$$

The temperatures within the solid region ($X(t) \le x$, $t > 0$) are obtained using:

$$T(x, t) = T_s + (T_m - T_s)\frac{\text{erfc}[(x/(2\sqrt{\alpha_s t})) - (1 - \mu)\nu\lambda]}{\text{erfc}(\mu\nu\lambda)} \quad (5)$$

where λ is the root of the transcendental equation:

$$\frac{St_l}{\lambda\ \exp(\lambda^2)\,\text{erf}(\lambda)} - \frac{St_s}{(\mu\nu\lambda)\ \exp[(\mu\nu\lambda)^2]\,\text{erfc}(\mu\nu\lambda)} = \sqrt{\pi} \quad (6)$$

where

$$\nu = \sqrt{\frac{\alpha_l}{\alpha_s}} \quad \text{and} \quad \mu = \frac{\rho_l}{\rho_s} \quad (7)$$

where α_s is the thermal diffusivity of a solid phase. ρ_l and ρ_s are the densities of the liquid and solid phase, respectively.

4. Modelling results

The thermal properties of paraffin wax, having approximately the same melting point as Fluka 76228, have been employed in this analytical analysis [17]. Table 1 shows the thermal properties of paraffin wax and the thermal diffusivities are calculated using:

$$\text{Thermal diffusivity } (\alpha) = \frac{\text{thermal conductivity } (k)}{\text{density } (\rho) \times \text{specific heat } (c)} \quad (8)$$

Fig. 3 shows the real paraffin wax dimensions for the Braille cell [13] and the micropipette [14,15], and the modelling dimensions for an ideal paraffin wax slab for performing calculations. The melting interface moves from bottom to top by means of heating. Since this modelling is calculated using Stefan's condition and Neumann's solution, there are several assumptions to simplify the problem:

Table 1
Thermal properties of paraffin wax [17]

Property	Value
Melting point (T_m) (°C)	47
Density (kg/m^3)	
Solid (ρ_s)	818
Liquid (ρ_l)	760
Latent heat (L) (J/kg)	266000
Thermal conductivity (W/m K)	
Solid (k_s)	0.24
Liquid (k_l)	0.24
Specific heat (J/kg °C)	
Solid (c_s)	2950
Liquid (c_l)	2510
Thermal diffusivity (m^2/s)	
Solid (α_s)	9.95E−8
Liquid (α_l)	1.3E−7

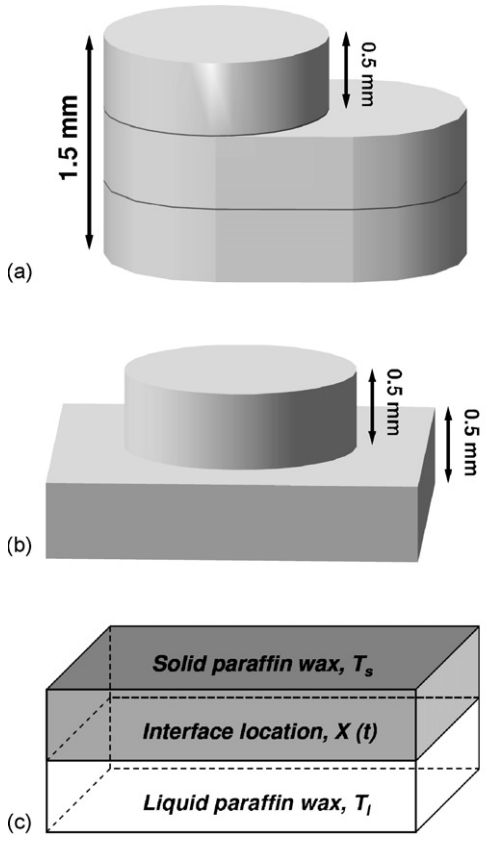

Fig. 3. Dimensions for paraffin wax microactuator: (a) Braille cell, (b) micropipette and (c) melting model of a paraffin wax slab for Neumann's solution.

(i) heat transfer is isotropic by conduction only, all other effects assumed negligible;
(ii) latent heat is constant;
(iii) phase change temperature is a fixed and known quantity (a property of the PCM);
(iv) interface thickness and structure are locally planar and sharp (a surface separating the phases) at the phase change temperature;
(v) thermal properties are constant in both solid and liquid phases;
(vi) the paraffin wax is homogenous and isotropic;
(vii) thermal resistance across the wall of the container is ignored.

Also, during melting, the solid paraffin wax can be pushed by expansion of the liquid paraffin wax, due to density differences ($\rho_l < \rho_s$). Therefore, the moving melting front (i.e. solid–liquid interface) can be affected by movement of the solid. The movement speed of the solid, $v(t)$, is obtained using [16]:

$$v(t) = \left[1 - \left(\frac{\rho_l}{\rho_s}\right)\right] X'(t) \tag{9}$$

where $X'(t)$ is the moving speed of the melting front. The movement speed of the solid is proportional to the moving speed of the melting front, with the constant $0 \leq 1 - (\rho_l/\rho_s) < 1$. Eq. (9) shows that the movement speed of the solid is slower than that of the melting front. Therefore, the effect of the movement of the solid paraffin wax during melting can be ignored in this analysis.

Table 2
Actuation data for the Braille cell and micropipette microactuators

	Actuation response time (s)	Initial temperature of solid paraffin wax (T_s) (°C)
Braille cell	42	30
Micropipette	10	30

In order to investigate the modelling of the Braille cell and the micropipette, their measured actuation data were taken, as shown in Table 2. Here, λ was obtained using the transcendental Eq. (6). Fig. 4 shows the variations of λ with increasing temperature (T_l) of the infinitesimally thin layer of liquid paraffin wax for an initial solid paraffin wax temperature (T_s) of 30 °C. In this research, the initial temperature of the solid paraffin wax was taken to be 30 °C, which is slightly higher than room temperature. This is because the actuation time was determined by taking an average value of many repeated actuation measurements at the given DC bias. Therefore, the paraffin wax did not have the chance to cool down to room temperature.

With λ derived, the location of a melting interface can be calculated as a function of time. Because the heights of the microactuators for the Braille cell and micropipette are 1.5 and 1.0 mm, respectively, as shown in Fig. 3(a and b), the times when the melting interfaces are passing the lengths of 1.5 and 1.0 mm, respectively, are regarded as the times when the paraffin wax of the microactuator fully melts. Therefore, these interface passing times can be represented as the actuation times for the microactuators. Interface locations against time were compared with the measured actuation times of the Braille cell and micropipette microactuators.

In practice, the actuation times for these two microactuators were measured by visual observation of the actuation height under a conventional optical microscope. The actuation time was recorded as the time taken for the paraffin wax microactuators to reach the maximum deflection height under DC bias.

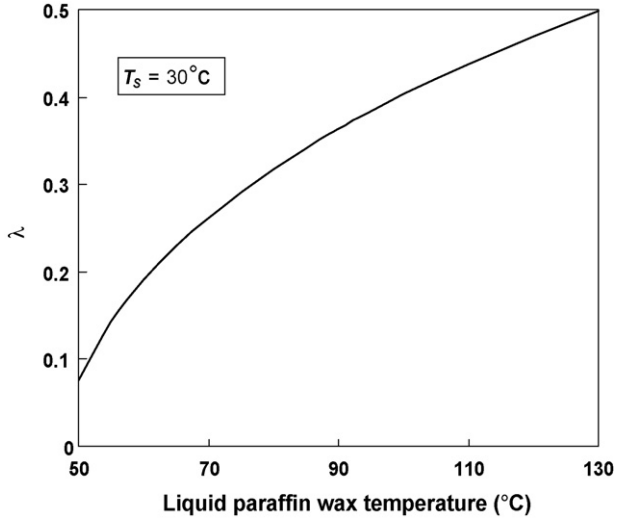

Fig. 4. Variation of λ for increasing liquid paraffin wax temperatures (T_l).

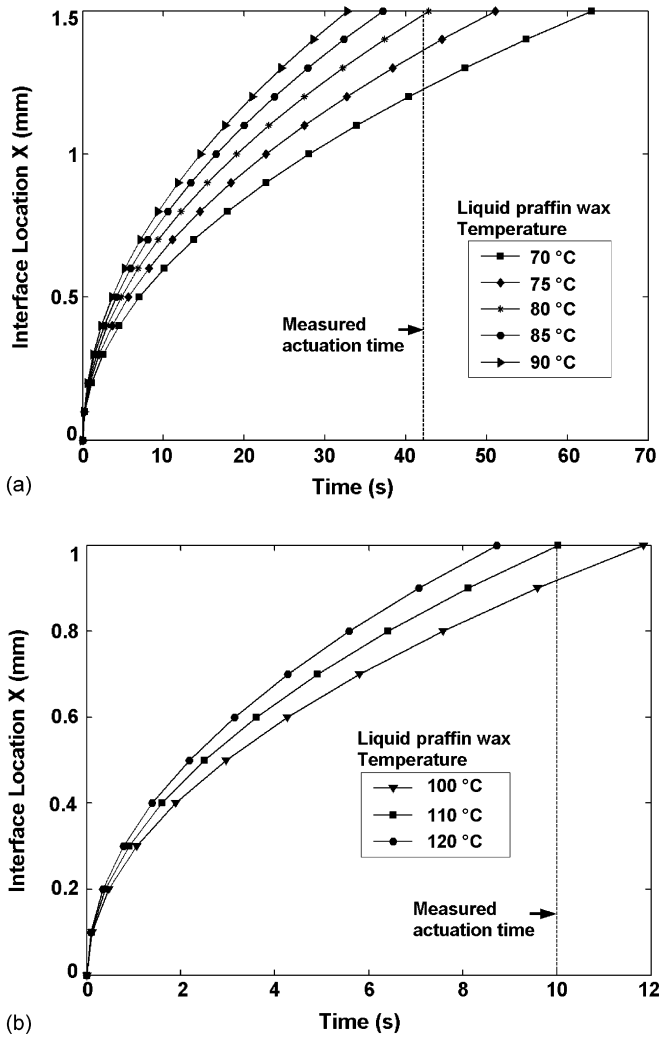

Fig. 5. Location of solid–liquid interface against time, for various liquid paraffin wax temperatures (T_l): (a) Braille cell and (b) micropipette.

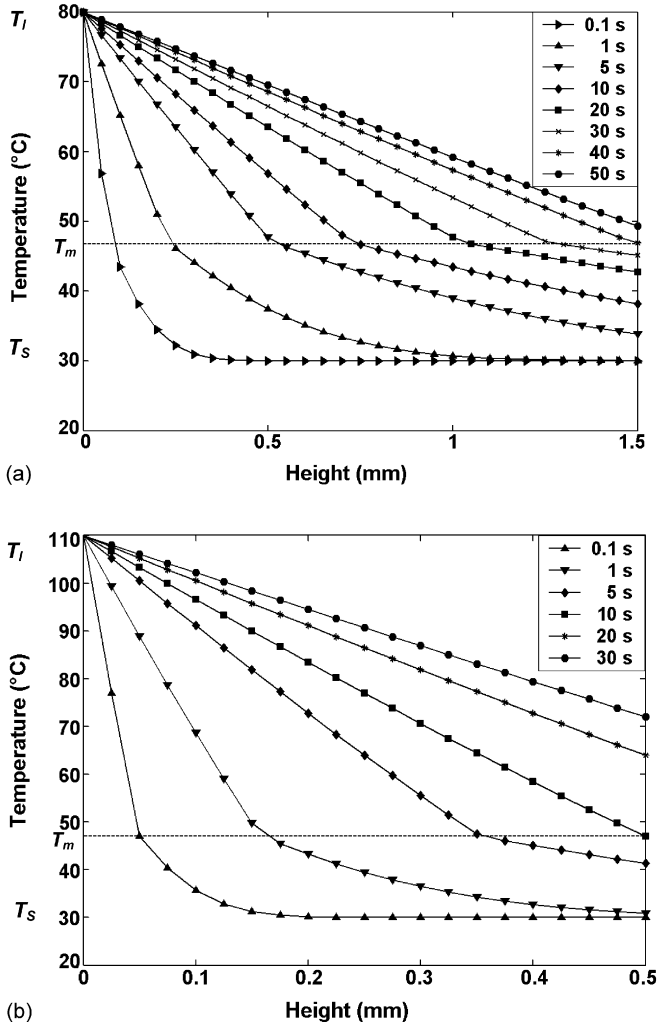

Fig. 6. Temperature profiles against paraffin wax height, for variations in time: (a) Braille cell and (b) micropipette.

For the Braille cell, the profile of interface locations calculated using λ at $T_l = 80\,^{\circ}C$, is close to the measured melting process actuation time of about 42 s, as shown in Fig. 5(a). This suggests that the temperature of the infinitesimally thin layer of theoretical liquid paraffin wax at the microheater is maintained at about 80 °C, during melting. Similarly, for the micropipette's microactuator, the calculated melting interface passing time, obtained using λ at $T_l = 110\,^{\circ}C$ gives the measured melting time of about 10 s, as shown in Fig. 5(b). The temperature of the infinitesimally thin layer of theoretical liquid paraffin wax at the microheater is about 110 °C.

The different actuation times for the Braille cell and micropipette microactuators are due to the different temperatures of the infinitesimally thin layer of theoretical liquid paraffin wax (T_l) at the microheater. In the actual melting processes, within the microactuators, the different actuation times are due to the differences in paraffin wax dimensions, as illustrated in Fig. 3 and different microheater designs. If the paraffin wax dimensions and the temperatures of the microheaters within a container are different, the actuation times and melting processes would be expected to be different. There may also be a contribution due to unwanted trapped air bubbles, as shown Fig. 2, introduced during microfabrication. Unfortunately, the effect of air bubbles is very difficult to quantify.

Using λ derived for the Braille cell's microactuator at $T_l = 80\,^{\circ}C$, temperature profiles inside the paraffin wax during the melting process were calculated. Fig. 6(a) shows temperature profiles against height for paraffin wax at different time intervals. At the time point of 0.1 s after melting commences, almost all the paraffin wax is still in a solid state (i.e. under the melting point). While, after about 40 s, all the paraffin wax has melted, because all the paraffin wax has been heated above its melting point.

The temperature profiles for the paraffin wax within the micropipette were also calculated, using λ obtained at $T_l = 110\,^{\circ}C$, as shown in Fig. 6(b). At approximately 10 s after melting, all the paraffin wax has melted.

Fig. 7 shows temperature profiles against time, for variations in paraffin wax height for the Braille cell and micropipette microactuators. With the Braille cell microactuator, the paraffin wax at a distance of 0.1 mm from the microheater melts within a few seconds after heating. However, the top of this microac-

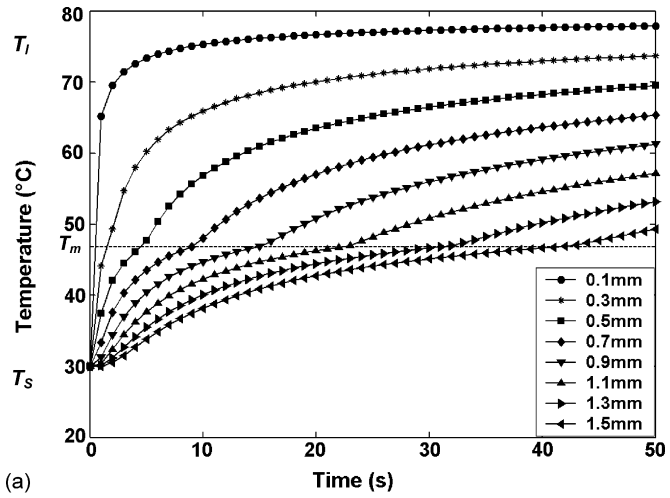

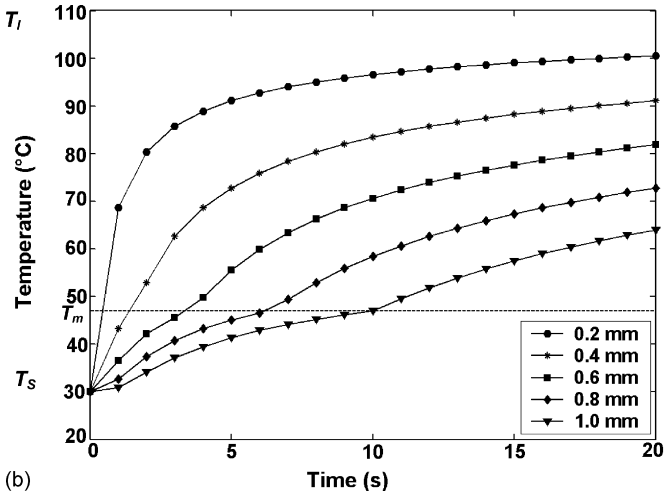

Fig. 7. Temperature profiles against time, for variations in paraffin wax height: (a) Braille cell and (b) micropipette.

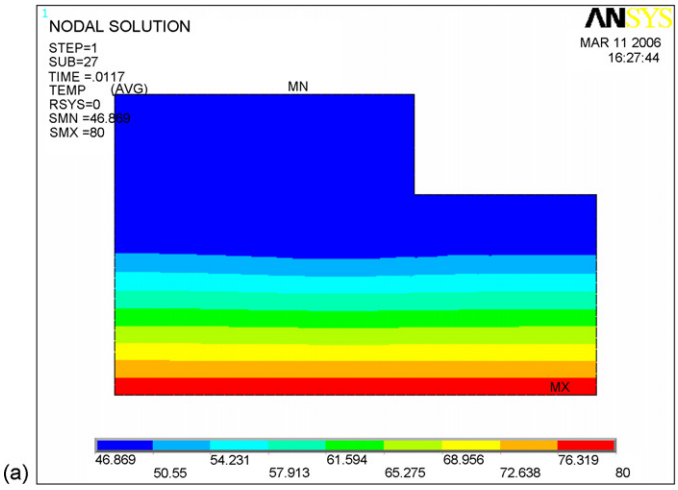

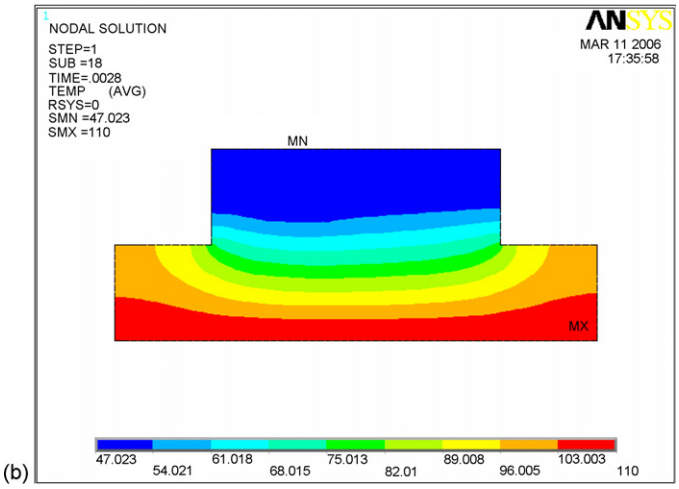

Fig. 8. Temperature distribution within paraffin wax: (a) the Braille cell after 42 s and (b) micropipette after 10 s.

tuator at a distance of 1.5 mm from the microheater is reached at its melting point after about 40 s, as illustrated in Fig. 7(a). For the paraffin wax within the micropipettes, the melting of the top paraffin wax of its microactuator takes approximately 10 s, as shown in Fig. 7(b).

The analytical modelling agrees with the measured actuation times of the Braille cell and the micropipette. With this analysis, it has been found that the actuation response time is affected by the temperature of the infinitesimally thin layer of liquid paraffin wax for the given thermal conditions. The effective heating of the infinitesimally thin layer of liquid paraffin wax at the initial state is important to reduce the response times of the microactuators. In order to heat efficiently, improvements in the microheater design and thermal management are needed. This is now possible with the characterization process described here.

5. Comparison with FEM results

In order to independently evaluate the analytical results, they were compared through simulations using finite element method (FEM) simulations, implemented in the widely used and commercially available software ANSYS. The FEM simulations were performed with paraffin wax dimensions given in Fig. 3(a and b). For the melting interface location, the position of the melting point at 47 °C was regarded as the location of the melting interface within the paraffin wax for the Braille cell and micropipette. Fig. 8(a and b) shows temperature contours within the paraffin wax after 42 and 10 s, respectively, with effectively non-thermal short circuit boundary conditions.

In addition, Fig. 9 shows the temperature distribution along the length of the paraffin wax and the containers in a more realistic scenario. The temperature distributions for paraffin wax within the containers are now different from the results given in Fig. 8. This is because the paraffin wax makes contact with the silicon container side walls and the bottom glass substrate, which act as effective thermal short circuits. It can be seen that a large amount of heat energy is conducted through the silicon walls and glass substrate.

With the Braille cell and micropipette, the final passing times for the melting interface are almost identical to the times from the analytical results, at the infinitesimally thin layer of theoretical

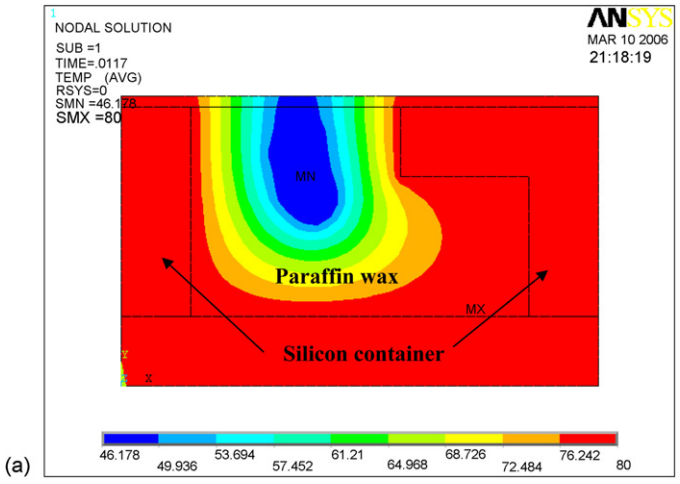

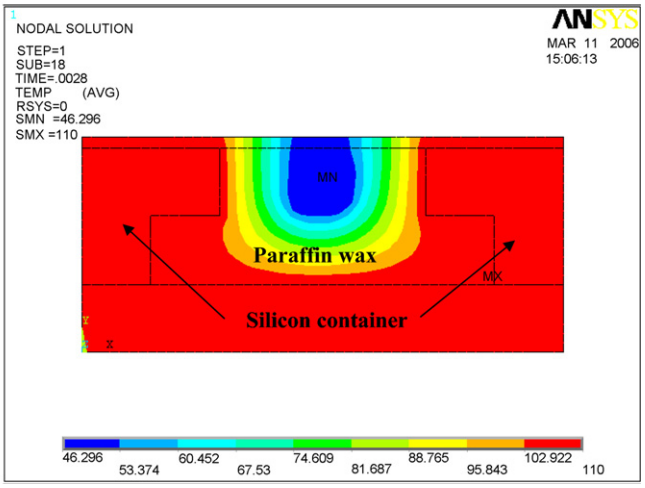

Fig. 9. Temperature distribution along the length of the paraffin wax and the containers with a thermal short circuit: (a) the Braille cell after 42 s and (b) micropipette after 10 s.

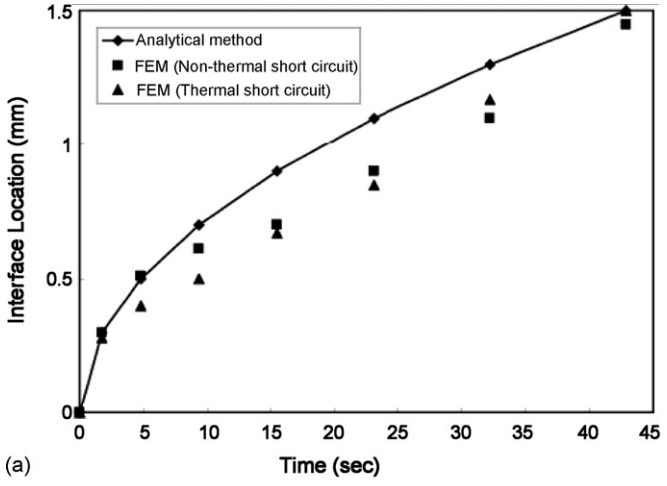

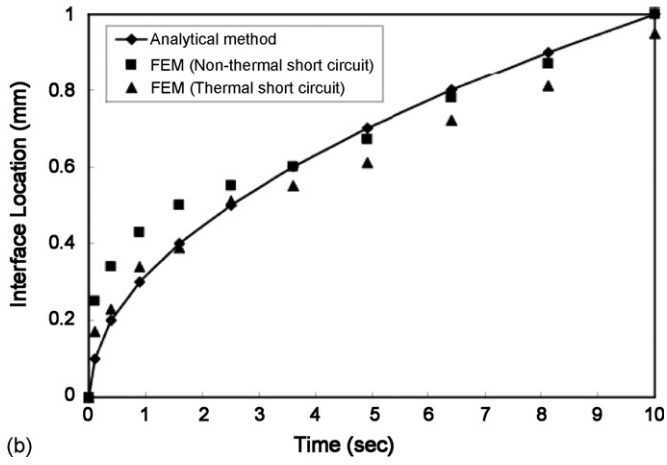

Fig. 10. Comparison of the analytical method, FEM simulations with a non-thermal short circuit and FEM simulations with a thermal short circuit for the location of the solid–liquid interface against time: (a) Braille cell and (b) micropipette.

liquid paraffin wax temperatures of 80 and 110 °C, respectively, as shown in Fig. 10. However, with the FEM results with a non-thermal short circuit and an effective thermal short circuit, the paths of the melting interface against time deviate from the analytical results in both the Braille cell and the micropipette cases, but not significantly.

The temperature profiles within the paraffin wax were also simulated using FEM with a non-thermal short circuit. Fig. 11(a) shows a comparison of the temperature profiles at the melting times of 1, 10 and 42 s for the Braille cell. The results from both the analytical method and FEM simulations show that the final melting times are very close to 42 s. However, the temperature profiles, obtained using FEM, do not always exactly match with the analytical results. With the micropipette on the melting times of 1, 5 and 10 s, the final melting time of the FEM simulations at 10 s is very close to the result from the analytical method. However, again the temperature profiles within the paraffin wax deviate from each other, as shown in Fig. 11(b).

Deviation in results from the analytical method, by FEM simulations, can be understood by considering the differences in which the calculations are performed. The final actuation times (or melting times) with the analytical method and the FEM simulations are very close, because the total heat energy required is almost identical to that needed to melt the given dimensions of paraffin wax. However, the modes of heat energy transfer are different. With the analytical method, the heat transfer is affected by the thermal diffusivity of the solid and liquid paraffin wax. The thermal diffusivities have different values between solid and liquid, as shown in Table 1. However with FEM, calculations are performed using enthalpy ($H = U + PV$, U is the internal energy of the system, P the pressure of the system and V is the volume), density and thermal conductivity. With our analytical modelling, the value of thermal conductivity was made identical for both solid and liquid phases of the paraffin wax.

The enthalpy–temperature relationship is expressed by:

$$H_s = \int_{30}^{T_m} c_s \, dT, \quad T \leq T_m, \text{ solid phase} \tag{10}$$

From Eq. (10), the enthalpy for the solid phase paraffin wax, for temperatures between 30 and 47 °C (melting point), is

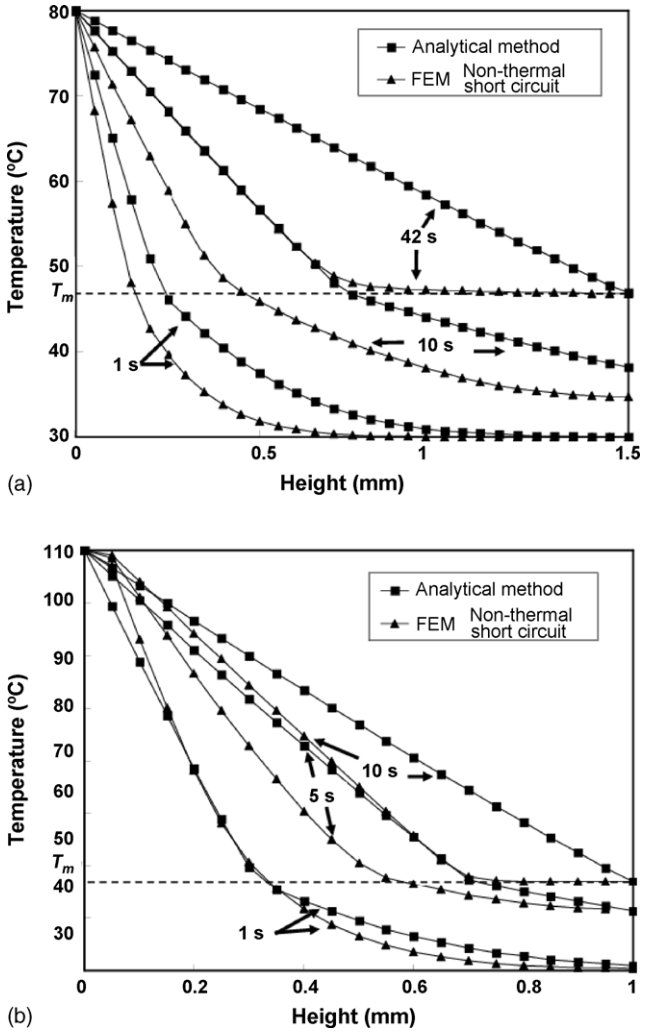

Fig. 11. Comparison of the analytical method and FEM simulations with a non-thermal short circuit for the temperature profiles against paraffin wax height, for variations in time: (a) Braille cell and (b) micropipette.

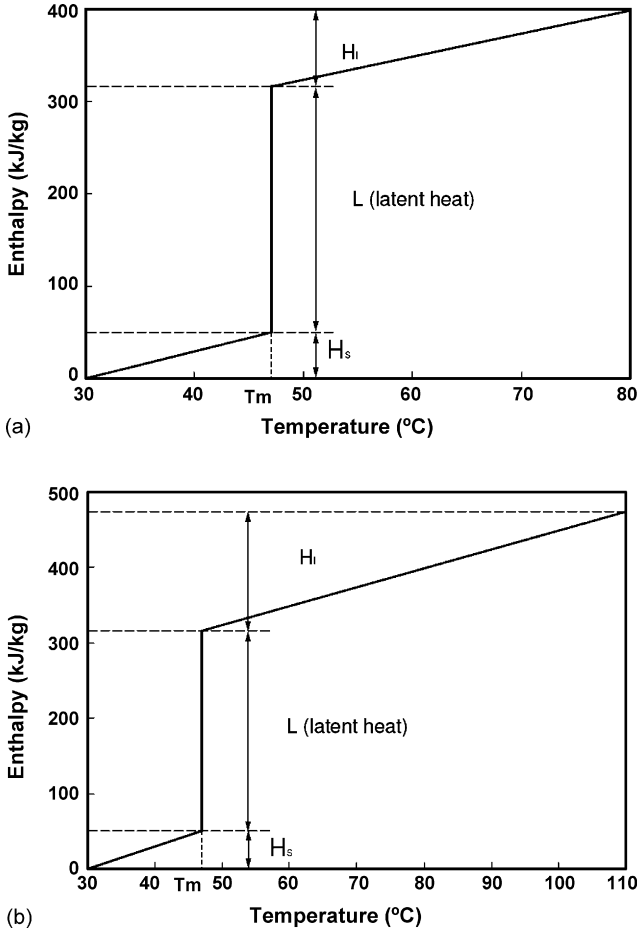

Fig. 12. Required total enthalpy of the paraffin wax for FEM simulations: (a) Braille cell and (b) micropipette.

50.15 kJ/kg for both the Braille cell and micropipette.

$$H_l = \int_{T_m}^{T} c_l \, dT, \quad T > T_m, \text{ liquid phase} \tag{11}$$

From Eq. (11), the enthalpy for the liquid phase paraffin wax is 82.83 kJ/kg, for temperatures between 47 °C (melting point) and 80 °C, for the Braille cell; and is 158.13 kJ/kg, for temperatures between 47 °C (melting point) and 110 °C, for the micropipette.

Therefore, total enthalpy (heat energy) for a temperature (T) is:

$$H_{total} = H_s + L + H_l \tag{12}$$

where L is latent heat (266 kJ/kg). With Eq. (12), the total enthalpy for the paraffin wax is 50.15 + 266 + 82.83 = 398.98 kJ/kg for the Braille cell; and is 50.15 + 266 + 158.13 = 474.28 kJ/kg for the micropipette, as shown in Fig. 12.

The total amount of enthalpy for melting the paraffin wax is fixed to the given dimensions. Therefore, the values for the final melting times and the final melting interface positions within the paraffin wax can be almost identical in both the analytical method and FEM simulations. Since the paths of the melting interface locations and temperature profiles within the paraffin wax are determined by the thermal diffusivity and thermal conductivity, the results can be different between the analytical method and FEM simulations. In real melting processes, the thermal transfer within paraffin wax is different for the solid and liquid phases. Therefore, the results from our analytical method are expected to be more realistic, when compared to those obtained from ANSYS simulations, because we use different values for the thermal diffusivities for both phases.

6. Conclusions

The melting process of the paraffin wax within the Braille cell and the micropipette has been analyzed using Stefan's problem and Neumann's solution. This analytical solution gives useful information on the location of the melting front for a given melting time, and on the temperature profiles within the paraffin wax during melting. Using the actual measured actuation response times for the Braille cell and micropipette microactuators (approximately 42 and 10 s, respectively), λ was calculated.

According to λ, the temperatures of the infinitesimally thin layers of theoretical liquid paraffin wax at the microheaters are approximately 80 and 110 °C, for the Braille cell and

micropipette, respectively, during the melting process. These infinitesimally thin layers of liquid paraffin wax temperatures give realistic results for the temperature profile within the paraffin wax during melting.

Also, using numerical FEM with non-thermal short circuit and effective thermal short circuit boundary conditions, the melting process was simulated independently. The final melting times are almost identical to those from the analytical results. The FEM results showed deviations in the paths of the interface locations and temperature profiles within the paraffin wax, due to differences in the calculations. The results from our analytical method are expected to be closer to the actual melting process. Moreover, this analytical modelling approach for the melting process of paraffin wax can provide valuable insight for designing optimal electrothermal hydraulic microactuators using PCMs and their operating actuation characteristics.

Acknowledgements

The authors would like to acknowledge Dr. John P. Stagg for undertaking the DRIE, Dr. Munir M. Ahmad for his advice on materials for the fabrication and Dr. Nicholas Avlonitis for his advice on numerical analysis. Finally, we wish to thank Professor P.D. Prewitt (Birmingham) and the late Dr. D.F. Moore (Cambridge) for their invaluable suggestions.

References

[1] S.F. Tibbitts, High-output paraffin linear motors: utilization in adaptive systems, in: SPIE, Proceedings, vol. 1543, 1991, pp. 388–399.
[2] D.E. Dowen, Design and implementation of a paraffin based micropositioning actuator, in: SPIE, vol. 3132, 1997, pp. 127–134.
[3] N. Kabei, M. Kosuda, H. Kagamibuchi, R. Tashiro, H. Mizuno, Y. Ueda, K. Tsuchiya, A thermal-expansion-type microactuator with paraffin as the expansive material, JSME Int. J., Ser. C 40 (4) (1997) 736–742.
[4] E.T. Carlen, C.H. Mastrangelo, Electrothermally activated paraffin microactuators, J. MEMS 11 (June (3)) (2002) 165–173.
[5] L. Klintberg, M. Karlsson, L. Stenmark, J.-Å. Schweitz, G. Thornell, A large stroke, high force paraffin phased transition actuator, Sens. Actuators A 96 (2002) 189–195.
[6] L. Klintberg, M. Svedberg, F. Nikolajeff, G. Thornell, Fabrication of a paraffin actuator using hot embossing of polycarbonate, Sens. Actuators A 103 (2003) 307–316.
[7] L. Klintberg, M. Karlsson, L. Stenmark, G. Thornell, A thermally activated paraffin-based actuator for gas-flow control in a satellite electrical propulsion system, Sens. Actuators A 105 (2003) 237–246.
[8] P. Selvaganapathy, E.T. Carlen, C.H. Mastrangelo, Electrothermally actuated inline microfluidic valve, Sens. Actuators A 3647 (2003) 1–8.
[9] E.T. Carlen, C.H. Mastrangelo, Surface micromachined paraffin-actuated microvalve, J. MEMS 11 (October (5)) (2002) 408–420.
[10] M. Lehto, R. Boden, U. Simu, K. Hjort, J.-A. Schweitz, Printed circuit board paraffin actuators for disposable microfluidic systems, in: Actuators 2004, June 14–16, 2004, pp. 220–223.
[11] R. Boden, M. Lehto, U. Simu, G. Thrnell, K. Hjort, J.-A. Schweitz, A polymeric paraffin micropump with active valves for high-pressure microfluidics, in: Transducers'05, Seoul, Korea, June 5–6, 2005.
[12] H. Yousef, M. Lehto, T. Jaderblom, I. Enculescu, K. Hjort, A device integrating paraffin microactuator, fluidic compartment and microneedle array for fluidic injection or sampling, 9th Int. Conf. Miniaturized Syst. Chem. Life Sci. (μTAS), Boston, MA, USA, October 9–13, 2005.
[13] J.S. Lee, S. Lucyszyn, A micromachined refreshable Braille cell, IEEE/ASME J. Microelectromech. Syst. 13 (4) (2005) 673–682.
[14] J.S. Lee, S. Lucyszyn, Bulk-micromachined hydraulic microactuator, in: ICMAT-2005, Proceedings of Symposium F, 2005, pp. 115–118.
[15] J.S. Lee, S. Lucyszyn, Design and pressure analysis for bulk-micromachined electrothermal hydraulic microactuator using PCM, Sens. Actuators A: Phys., accepted for publication (Special issue).
[16] V. Alexiades, A.D. Solomon, Mathematical Modelling of Melting and Freezing Processes, Hemisphere Publishing Corporation, USA, 1993.
[17] P. Broussenau, M. Lacroix, Numeriacl simulation of a multi-layer latent heat thermal energy storage system, Int. J. Energy Res. 22 (1998) 1–15.

Biographies

Jun Su Lee was born in South Korea in 1970. He received the MSc degree in metallurgical engineering from Yonsei University, Seoul, in 1999. From 2000 to 2001, he worked as an intern researcher, within the Metal Processing Research Centre of the Materials Science and Technology Division in the Korea Institute of Science and Technology (KIST, Seoul). In 2006 he received his PhD degree in electrical and electronic engineering at Imperial College London, UK. His current interests are in intelligent materials for MEMS and microfluidic devices.

Stepan Lucyszyn joined Imperial College in June 2001, as a senior lecturer within the Optical and Semiconductor Devices Group. Prior to this, he was a senior lecturer at the University of Surrey. He represents Imperial within the European Union's Framework VI Network of Excellence on Advanced MEMS for RF and Millimeter Wave Communications (AMICOM). During the summer of 2002, Dr. Lucyszyn worked as a guest researcher, within the MEMS laboratory of the National Institute of Advanced Industrial Science and Technology (Tsukuba, Japan). In 2004, he published a review paper on RF MEMS technology, which won an IEE Premium Award in 2005. More recently, in October 2005, he gave an invited presentation of his RF MEMS research activities to a NATO Workshop. In November 2005, he was appointed an associate editor and serves as a member of the editorial board for the IEEE/ASME Journal of Microelectromechanical Systems. To date, Dr. Lucyszyn has (co-)authored over 100 publications in areas of applied physics and engineering. In 2005, he was elected fellow of the Institution of Electrical Engineers and a fellow of the Institute of Physics.